



Cite this: *CrystEngComm*, 2020, 22, 164

Received 5th October 2019,
Accepted 25th November 2019

DOI: 10.1039/c9ce01572h

rsc.li/crystengcomm

Facile fabrication of titanosilicate zeolites with an unprecedented wide range of Si/Ti ratios by employing transition metal dichalcogenides as metal precursors†

Liangliang Liu, Yanwei Sun, Yi Liu, Gaohong He  and Yi Liu *

In this study, layered JDF-L1 zeolites with Si/Ti ratios down to 2.0 were *in situ* synthesized by using transition metal dichalcogenides as metal precursors. Employment of layered TiS₂ as metal precursors led to an unprecedented wide range of Si/Ti ratios and effective suppression of the formation of a TiO₂ impurity phase.

Relying on the presence of versatile Ti species within the framework, titanosilicate zeolites have gained widespread attention in the fields of catalysis, adsorption, separation and ion exchange.¹ Facile control of contents, locations and coordination states of Ti species represents one of the most significant challenges for titanosilicate zeolite synthesis, which requires stringent control over the nucleation and growth kinetics.² At present, manipulation of the microstructure and chemical composition (*i.e.*, Si/Ti ratio) of titanosilicate zeolites is still based on trial-and-error, owing to the fast hydrolysis of commonly used titanium precursors (such as TPOT, TBOT or TiCl₄).^{1e} In addition, since common titanium precursors are vulnerable to water vapour even upon transient exposure to air, their storage, transportation and utilization conditions must be accurately controlled to prevent the formation of any undesired by-products (like TiO₂) and the incorporation of extra-framework Ti species into the framework.

The use of moisture/water stable titanium precursors represents an effective approach to overcome the above challenges.³ Heterometallic single-source precursors have been employed to form mesophases. This approach not only afforded desired compositions in preparation of mesoporous nanocrystals but also effectively alleviated undesired metal segregation.^{3d} It was therefore anticipated that the slow hydrolysis rate of titanium precursors under hydrothermal

conditions enabled us to precisely tailor the nucleation and growth kinetics so that their microstructures and chemical compositions could be accurately controlled; in addition, the formation of impurity phases may be effectively suppressed. In this regard, TiO₂ has been considered as a potential candidate for water stable titanium precursors which, however, is still far from maturity.^{3a,4,5} For instance, Xin *et al.* successfully prepared TS-1 zeolites with TiO₂ precursors; nevertheless, a complicated pretreatment process was required to prevent the formation of extra-framework Ti species.⁴ Recently Ti-CHA zeolites were synthesized from TiO₂ precursors which, however, could not be completely converted even under harsh hydrothermal conditions.⁵ Therefore, facile preparation of qualified titanosilicate zeolites from moisture/water stable titanium precursors remained a great challenge.

In recent decades transition metal dichalcogenides (TMDCs) as emerging two-dimensional layered materials have attracted tremendous attention.⁶ Our recent research indicated that TMDCs could serve as competent metal sources for metal organic frameworks (MOFs), owing to their outstanding air/moisture stability, unique layered structure and decent M–X bonding strength.⁷ The competence of TMDCs as metal precursors for zeolites (like titanosilicate zeolites), however, has not been explored so far. In comparison with Ti-MOFs, synthesis of qualified titanosilicate zeolites requires not only uniform distribution of Ti species within the framework, but also effective suppression of the formation of undesired impurity phases. In addition, both their microstructures and chemical compositions should be facilely adjusted.

JDF-L1 zeolites as a representative of titanosilicate zeolites consist of unique TiO₅ square pyramids, each of which is linked to SiO₄ tetrahedra forming continuous sheets.⁸ JDF-L1 zeolites possess a typical layered structure with an in-plane pore size of ~3 Å, making them promising candidates for H₂ selective adsorbents or membranes.⁹ In this study, we reported facile hydrothermal synthesis of JDF-L1 zeolites by

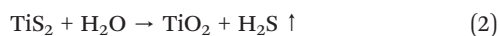
State Key Laboratory of Fine Chemicals, School of Chemical Engineering, Dalian University of Technology, Dalian 116023, P. R. China.

E-mail: diligenliu@dlut.edu.cn

† Electronic supplementary information (ESI) available. See DOI: 10.1039/c9ce01572h

employing layered TiS_2 as a titanium precursor and a related mechanism associated with the formation of JDF-L1 zeolites was hypothesized (Scheme 1). It was noted that the prepared JDF-L1 zeolites exhibited a record-breaking framework Ti content (Si/Ti ratio down to 2.0); moreover, besides JDF-L1 zeolites, diverse titanosilicate zeolites (like ETS-4) could be facily prepared from layered TiS_2 precursors therefore demonstrating the great potential of TMDCs as precursors for transition-metal containing zeolites.

Layered TiS_2 -derived JDF-L1 zeolites were prepared by facile hydrothermal growth using a precursor solution with a molar composition of $4.5\text{Na}_2\text{O}:5.5\text{SiO}_2:\text{TiO}_2:258\text{H}_2\text{O}$ (detailed experimental procedures are presented in SI-1, ESI†). The whole reaction can be expressed as eqn (1):



It was noted that accompanied with the formation of JDF-L1 zeolites, other undesired side products (like TiO_2) may also be generated under hydrothermal conditions (eqn (2), details are shown in the ESI†). Nevertheless, as will be shown below, the formation of a TiO_2 impurity phase could be effectively avoided when layered TiS_2 is employed as a titanium precursor. Moreover, spontaneous phase segregation of H_2S from the aqueous reaction medium favored the complete conversion of layered TiS_2 precursors.

As shown in the XRD patterns (Fig. 1a), diffraction peaks derived from products matched well with those reported in the literature,⁸ therefore indicating that obtained products indeed belonged to pure JDF-L1 phase. The SEM image further indicated that square plate-shaped JDF-L1 crystals with grain sizes ranging from 5 to 10 μm tended to stack together along the largest facets (Fig. 1b). In addition, prepared JDF-L1 zeolites exhibited type II isotherms with low N_2 adsorption capacity since their pore size was too small to allow the entrance of N_2 molecules (*ca.* 3 \AA , Fig. 1c).¹⁰ As a result, the BET surface area and pore volume were calculated to be only $14.32\text{ m}^2\text{ g}^{-1}$ and $0.0570\text{ cm}^3\text{ g}^{-1}$, respectively. As indicated in the UV-vis spectrum (Fig. 1d), prepared JDF-L1 crystals exhibited an absorption peak around 230 nm, which could be assigned to five-coordinated Ti species, which was unique for JDF-L1 zeolites.^{8a} Simultaneously, characteristic diffraction peaks derived from hexa-

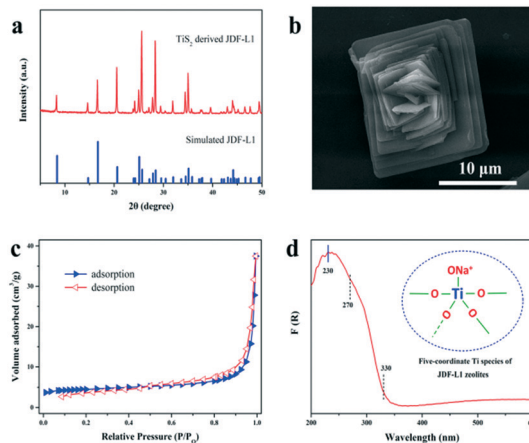
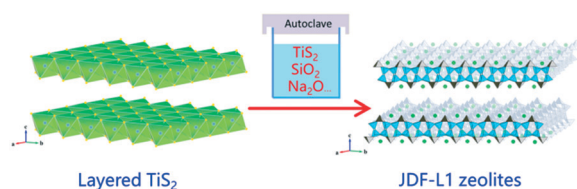


Fig. 1 (a) XRD patterns, (b) SEM image, (c) N_2 adsorption/desorption isotherms and (d) DR UV-vis spectrum of JDF-L1 titanosilicate zeolites obtained at 200 $^\circ\text{C}$ (inset: five-coordinate Ti species of JDF-L1 zeolites).

coordinated Ti (270 nm) or anatase (330 nm) could not be discerned,¹¹ suggesting that Ti species have been fully incorporated into the framework. The five-coordination site for Ti species could be further identified by FT-IR spectroscopy (Fig. S1a, ESI†).¹² TGA results indicated that prepared JDF-L1 crystals maintained a negligible weight loss up to 780 $^\circ\text{C}$ under atmospheric conditions (Fig. S1b, ESI†) therefore indicating a high thermal stability. In addition, no distinct changes in crystallinity and morphology were observed for JDF-L1 zeolites even under harsh alkaline conditions, which was quite advantageous for their practical applications (Fig. S2, ESI†).

In the next step, the structural evolution process of JDF-L1 zeolites under hydrothermal conditions was systematically investigated. Pristine layered TiS_2 exhibited a typical sheet-like morphology (Fig. 2a, 3a and S3, ESI†). Upon hydrothermal crystallization for only 1 h, diffraction peaks



Scheme 1 Synthesis of JDF-L1 titanosilicate zeolites from layered TiS_2 (left: blue, Ti atoms; yellow, S atoms; right: grey, TiO_5 square pyramids; dark green, SiO_4 tetrahedra; green, Na^+ ions; H_2O molecules have been omitted for clarity).

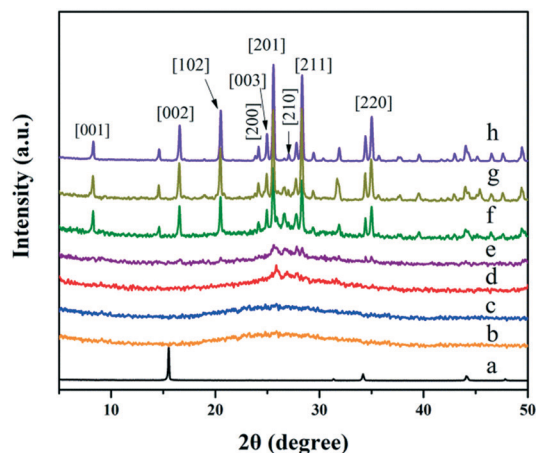


Fig. 2 XRD patterns of JDF-L1 zeolites obtained at 200 $^\circ\text{C}$ at different crystallization times: (a) 0 h – TiS_2 , (b) 1 h, (c) 8 h, (d) 18 h, (e) 24 h, (f) 36 h, (g) 48 h and (h) 72 h.

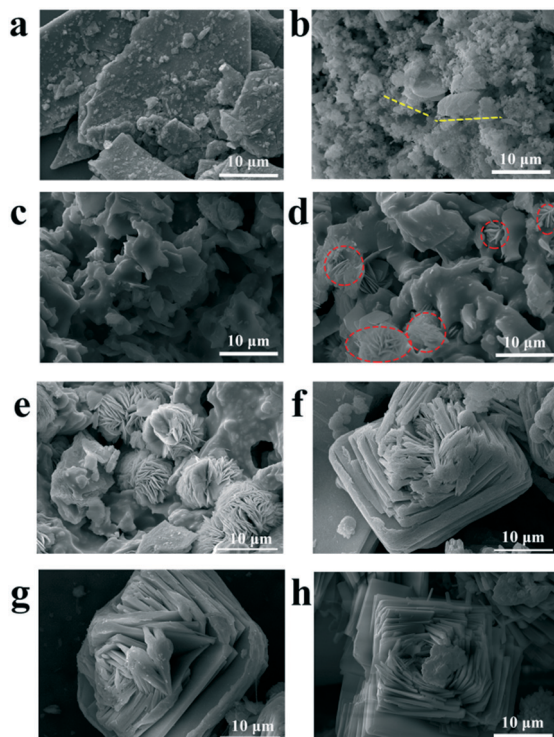


Fig. 3 SEM images of JDF-L1 titanasilicate zeolites obtained at 200 °C at different crystallization times: (a) 0 h – TiS₂, (b) 1 h, (c) 8 h, (d) 18 h, (e) 24 h, (f) 36 h, (g) 48 h and (h) 72 h.

derived from layered TiS₂ disappeared implying that it had been completely amorphized (Fig. 2b); simultaneously, the obtained solid products exhibited an irregular morphology, which was in accordance with their amorphous nature (Fig. 3b, S4 and S5, ESI†). Element analysis results indicated that the Si/Ti ratio reached 2.2 while the sulfur content decreased significantly (Fig. S6 and S7, ESI†). Simultaneously, the pH value also decreased since a substantial amount of OH⁻ anions had been consumed accompanying with rapid dissolution of solid precursors (Table S2, ESI†). Simultaneously, new bands appearing at 230 nm and 275 nm in the UV-vis absorption spectra could be assigned to the dehydrated Ti in the hydrophilic silica surface¹³ and incipient oligomerization Ti species (Fig. S8, ESI†).¹⁴ These results indicated the fast hydrolysis rates of layered TiS₂ precursors and gradual attachment of SiO₂ gels to the surface of layered TiS₂ precursors. After hydrothermal treatment for 8 h, the grain size of solid products became uniform (Fig. 3c) despite still being amorphous. Further prolonging the crystallization duration to 18 h led to the generation of weak diffraction peaks (25.7°) derived from JDF-L1 zeolites, implying that the nucleation of the JDF-L1 phase had occurred (Fig. 2d). SEM images further demonstrated that plate-like JDF-L1 nuclei had been generated and assembled into 2 μm-sized flower-like aggregates sparsely distributed on amorphous intermediates (Fig. 3d). Simultaneously, as shown by FT-IR, the appearance of a new band at 675 cm⁻¹, which could be assigned to symmetric

stretching vibrations of tetrahedral SiO₄ units,^{8b,12} also suggested the formation of JDF-L1 nuclei (Fig. S9, ESI†). Further prolonging the crystallization duration to 24 h led to the generation of a large amount of JDF-L1 crystals with a larger grain size (*ca.* 10 μm, Fig. 2e and 3e). During the time interval, the pH value slowly increased due to the gradual release of OH⁻ anions in the process of rearrangement of intermediate precursors (Table S2, ESI†). After hydrothermal treatment for 36 h, majority of amorphous gels had been converted to JDF-L1 zeolites with not only a larger grain size but also a well-developed morphology (Fig. 3f); nevertheless, a substantial amorphous phase still existed (Fig. S10, ESI†). The FT-IR spectra indicated that several characteristic bands associated with JDF-L1 zeolites appeared simultaneously (Fig. S9, ESI†). These results revealed that well-crystallized JDF-L1 zeolites had been formed. To quantify the phase change from amorphous precursors to crystalline JDF-L1 crystals, the relative crystallinity of JDF-L1 zeolites at different crystallization times was calculated. Fig. 4 shows that all the obtained solid precipitates exhibited low relative crystallinity in an early stage (0–2.8%). After hydrothermal reaction for 36 h, the relative crystallinity sharply increased to 39.7% which clearly indicated an abrupt phase change from amorphous precursors to crystalline JDF-L1 zeolites. Further prolonging the crystallization time to 72 h led to complete conversion of amorphous gels to JDF-L1 zeolites as was confirmed by XRD, SEM, FT-IR and relative crystallinity results (Fig. 2g and h, 3g and h, 4 and S4–S9, ESI†). In addition, the appearance of a new band located at 230 nm in the UV-vis spectra could be assigned to five-coordinated Ti species of JDF-L1 zeolites, while the absence of a band located at 330 nm further ruled out the formation of other impurity phases like TiO₂ (Fig. S8, ESI†).¹¹

The above experimental data inspired us to postulate a JDF-L1 zeolite formation mechanism. At an early stage, layered TiS₂ precursors were quickly amorphized upon nucleophilic attack and their surface was covered with SiO₂

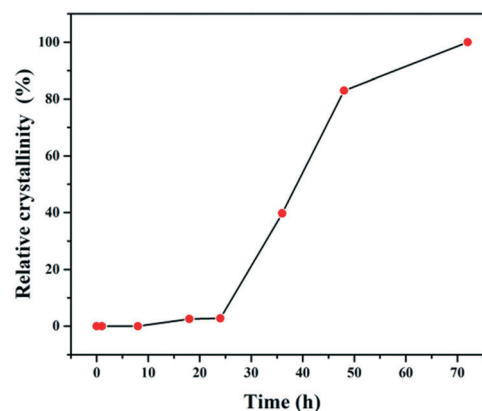


Fig. 4 Dependence of JDF-L1 zeolite relative crystallinity on crystallization time (relative crystallinity is based on the peak intensity in simulated XRD patterns, and the relative crystallinity of fully crystallized JDF-L1 zeolites synthesized at 200 °C for 72 h is designated as 100%).

gels. Consequently, nutrients located in amorphous gels were rearranged and then uniformly distributed under hydrothermal conditions. In the next step, JDF-L1 zeolites preferentially nucleated on the surface of solid amorphous gels since the concentration of nutrients at the solution–amorphous solid interface was the highest. Finally, JDF-L1 nuclei gradually grew larger, began to merge with each other and finally converted to well-developed JDF-L1 zeolites along with unceasing consumption of amorphous gel nutrients.

Possessing a wide range of Si/Ti ratios represents a critical issue for titanosilicate zeolites. In this study, Si/Ti ratios in both initial gels and corresponding JDF-L1 zeolites were measured. Our research indicated that prepared JDF-L1 zeolites maintained high phase purity and crystallinity within a broad range of Si/Ti ratios as was indicated in PXRD patterns (Fig. 5) and FT-IR spectra (Fig. S11, ESI†). Moreover, it was noted that the Si/Ti ratios of JDF-L1 zeolites increased with increasing Si/Ti ratios in initial gels firstly, reached a maximum value, and then decreased when the Si/Ti ratios in initial gels exceeded 6.0 (Table S3, ESI†). In particular, pure Ti-rich JDF-L1 zeolites with a Si/Ti ratio as low as 2.0 could be easily synthesized (Fig. 6). To the best of our knowledge, this represents the highest content of framework titanium compared with those of any JDF-L1 titanosilicate zeolites reported to date.^{8,10,12} It is anticipated that increasing the Ti content in the zeolite framework will enable further

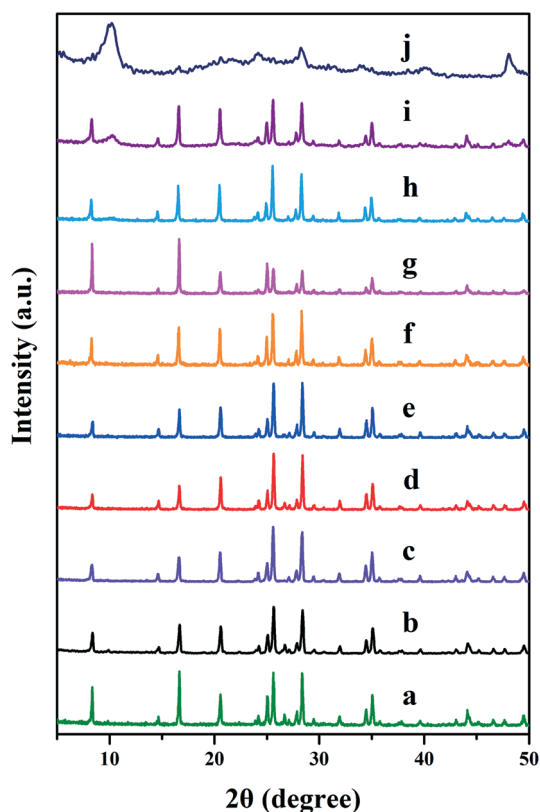


Fig. 5 XRD patterns of JDF-L1 zeolites obtained with various Si/Ti gel ratios: (a) 10.0, (b) 8.0, (c) 6.0, (d) 5.5, (e) 5.0, (f) 4.0, (g) 3.0, (h) 2.5, (i) 2.0 and (j) 1.5, respectively.

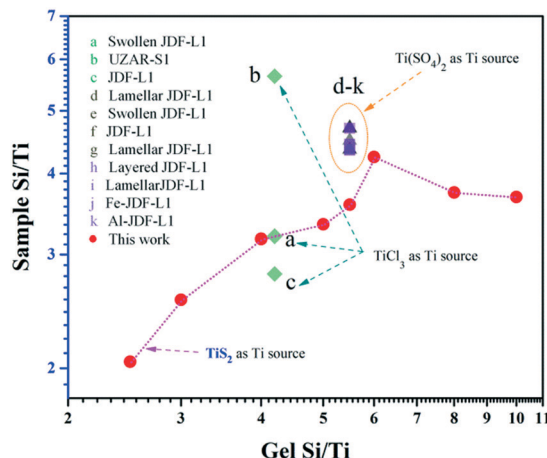


Fig. 6 Si/Ti molar ratios for JDF-L1 zeolites obtained at 200 °C with different initial gels (measured by ICP) and comparison with other JDF-L1 titanosilicate zeolites (the results are obtained from different Ti sources: a–c, TiCl_3 precursors;^{8f} d–k, $\text{Ti}(\text{SO}_4)_2$ precursors^{8i,10,12}).

enhancement of its stability and application performance, which is currently underway. In addition, it is interesting to note that although further decreasing Si/Ti ratios in initial gels (<2.5) inevitably led to the generation of an amorphous Ti-rich phase along with the formation of JDF-L1 zeolites, the generation of an undesired TiO_2 impurity phase was still effectively avoided, even though the reaction was thermodynamically favored (eqn (2), Fig. S12, ESI†). This represents an obvious advantage over the use of other common titanium precursors like TPOT and TiCl_4 .

To further verify the generality of this approach, herein we tried to prepare other titanosilicate zeolites like ETS-4 by using layered TiS_2 as a titanium precursor under hydrothermal conditions. As shown in Fig. 7, both the XRD pattern and SEM image of ETS-4 zeolites were in good agreement with those reported in the literature,¹⁵ therefore demonstrating that layered TiS_2 was potentially a qualified titanium precursor for diverse titanosilicate zeolites.

To summarize, in this study we presented a generalized approach to synthesize titanosilicate zeolites from layered TiS_2 precursors. Owing to their unique layered structure, decent bonding strength and high water stability, high-quality JDF-L1 zeolites could be facily synthesized *via in situ* hydrothermal treatment of layered TiS_2 precursors. A detailed investigation of the crystallization process enabled us to

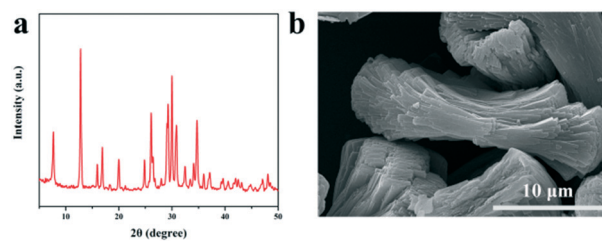


Fig. 7 (a) XRD pattern and (b) SEM image of ETS-4 titanosilicate zeolites.

propose a multi-step mechanism referring to JDF-L1 zeolite growth. More importantly, a record-breaking Si/Ti ratio (down to 2.0) in JDF-L1 zeolites was obtained. Besides JDF-L1 zeolites, layered TiS₂ could be used to synthesize diverse titanosilicate zeolites like ETS-4 so the toolbox for the preparation of qualified titanosilicate zeolites was greatly expanded. It was expected that with this method diverse transition-metal containing zeolites could be prepared with TMDCs as metal precursors.

The authors are grateful to the Liaoning Revitalization Talents Program (XLYC1807084), the National Natural Science Foundation of China (21176231), the Thousand Youth Talents Program and the Technology Innovation Team of Dalian University of Technology (DUT2017TB01) for the financial support.

Conflicts of interest

There are no conflicts to declare.

Notes and references

- (a) M. Moliner and A. Corma, *Microporous Mesoporous Mater.*, 2014, **189**, 31–40; (b) J. Přeck, P. Pizarro, D. P. Serrano and J. Áejka, *Chem. Soc. Rev.*, 2018, **47**, 8263–8306; (c) S. M. Kuznicki, V. A. Bell, S. Nair, H. W. Hillhouse, R. M. Jacobinas, C. M. Braunbarth, B. H. Toby and M. Tsapatsis, *Nature*, 2001, **412**, 720–724; (d) K. Popa and C. C. Pavel, *Desalination*, 2012, **293**, 78–86; (e) O. Oleksienko, C. Wolkersdorfer and M. Sillanpää, *Chem. Eng. J.*, 2017, **317**, 570–585.
- (a) W. Fan, R. Duan, T. Yokoi, P. Wu, Y. Kubota and T. Tatsumi, *J. Am. Chem. Soc.*, 2008, **130**, 10150–10164; (b) M. Signorile, V. Crocellà, A. Damin, B. Rossi, C. Lamberti, F. Bonino and S. Bordiga, *J. Phys. Chem. C*, 2018, **122**, 9021–9034; (c) W. O. Parker and R. Millini, *J. Am. Chem. Soc.*, 2006, **128**, 1450–1451.
- (a) X. Liu and J. K. Thomas, *Chem. Commun.*, 1996, 1435–1436; (b) X. Yang, J. L. Paillaud, H. F. W. J. Van Breukelen, H. Kessler and E. Duprey, *Microporous Mesoporous Mater.*, 2001, **46**, 1–11; (c) H. Horikawa, T. Iida, R. Osuga, K. Ohara, J. N. Kondo and T. Wakihara, *Cryst. Growth Des.*, 2018, **18**, 2180–2188; (d) M. A. Carreon, V. V. Gulians, Y. Li, A. R. Hughett, A. Dozier, G. A. Seisenbaeva and V. G. Kessler, *Eur. J. Inorg. Chem.*, 2006, **24**, 4983–4988.
- Y. Qi, C. Ye, Z. Zhuang and F. Xin, *Microporous Mesoporous Mater.*, 2011, **142**, 661–665.
- S. Imasaka, H. Ishii, J. Hayashi, S. Araki and H. Yamamoto, *Microporous Mesoporous Mater.*, 2019, **273**, 243–248.
- (a) M. Chhowalla, H. S. Shin, G. Eda, L. J. Li, K. P. Loh and H. Zhang, *Nat. Chem.*, 2013, **5**, 263–275; (b) Q. Lu, Y. Yu, Q. Ma, B. Chen and H. Zhang, *Adv. Mater.*, 2016, **28**, 1917–1933; (c) S. Manzeli, D. Ovchinnikov, D. Pasquier, O. V. Yazyev and A. Kis, *Nat. Rev. Mater.*, 2017, **2**, 17033; (d) X. Zhang, Z. Lai, Q. Ma and H. Zhang, *Chem. Soc. Rev.*, 2018, **47**, 3301–3338.
- (a) Y. Sun, S. Hu, C. Song, S. Miao, Z. Jiang, X. Jiang, J. Zhao, X. Guo and Y. Liu, *Chem. Commun.*, 2018, **54**, 3664–3667; (b) Y. Sun, Y. Liu, J. Caro, X. Guo, C. Song and Y. Liu, *Angew. Chem., Int. Ed.*, 2018, **57**, 16088–16093.
- (a) M. A. Roberts, G. Sankar, J. M. Thomas, R. H. Jones, H. Du, M. Fang, J. Chen, W. Pang and R. Xu, *Nature*, 1996, **381**, 401–404; (b) H. Du, M. Fang, J. Chen and W. Pang, *J. Mater. Chem.*, 1996, **6**, 1827–1830; (c) Z. Lin, J. Rocha, P. Brandão, A. Ferreira, A. P. Esculcas, J. D. P. De Jesus, A. Philippou and M. W. Anderson, *J. Phys. Chem. B*, 1997, **101**, 7114–7120; (d) S. Ferdov, V. Kostov-Kytin and O. Petrov, *Chem. Commun.*, 2002, 1786–1787; (e) C. Rubio, C. Casado, S. Uriel, C. Téllez and J. Coronas, *Mater. Lett.*, 2009, **63**, 113–115; (f) C. Rubio, C. Casado, P. Gorgojo, F. Etayo, S. Uriel, C. Téllez and J. Coronas, *Eur. J. Inorg. Chem.*, 2010, **1**, 159–163; (g) S. Ferdov, *CrystEngComm*, 2014, **16**, 4467–4471; (h) B. K. Yoo, Z. Su, J. M. Thomas and A. H. Zewail, *Proc. Natl. Acad. Sci. U. S. A.*, 2016, **113**, 503–508; (i) L. Zhang, J. Li, Y. Jin, S. Zhang, S. Sun and S. Zhao, *Mater. Lett.*, 2016, **176**, 219–222.
- (a) A. Galve, D. Sieffert, E. Vispe, C. Téllez, J. Coronas and C. Staudt, *J. Membr. Sci.*, 2011, **370**, 131–140; (b) S. Castarlenas, P. Gorgojo, C. Casado-Coterillo, S. Masheshwari, M. Tsapatsis, C. Téllez and J. Coronas, *Ind. Eng. Chem. Res.*, 2013, **52**, 1901–1907; (c) A. Galve, D. Sieffert, C. Staudt, M. Ferrando, C. Güell, C. Téllez and J. Coronas, *J. Membr. Sci.*, 2013, **431**, 163–170.
- L. Zhang, J. Han, Y. Jin, S. Zhang, S. Asaoka and S. Zhao, *Mater. Lett.*, 2016, **183**, 265–267.
- R. Bai, Q. Sun, Y. Song, N. Wang, T. Zhang, F. Wang, Y. Zou, Z. Feng, S. Miao and J. Yu, *J. Mater. Chem. A*, 2018, **6**, 8757–8762.
- L. Zhang, J. Han, L. Li, X. Zhao, S. Asaoka, S. Zhao and Y. Jin, *Eur. J. Inorg. Chem.*, 2016, **33**, 5185–5188.
- M. C. Capel-Sanchez, J. M. Campos-Martin, J. L. G. Fierro, M. P. De Frutos and A. Padilla Polo, *Chem. Commun.*, 2000, 855–856.
- L. Marchese, T. Maschmeyer, E. Gianotti, S. Coluccia and J. M. Thomas, *J. Phys. Chem. B*, 1997, **101**, 8836–8838.
- (a) S. Nair, H. K. Jeong, A. Chandrasekaran, C. M. Braunbarth, M. Tsapatsis and S. M. Kuznicki, *Chem. Mater.*, 2001, **13**, 4247–4254; (b) X. An, P. G. Ingole, W. K. Choi, H. K. Lee, S. U. Hong and J. D. Jeon, *J. Membr. Sci.*, 2017, **531**, 77–85.